Journal of Power Sources 240 (2013) 644–652

Contents lists available at SciVerse ScienceDirect

Journal of Power Sources

journal homepage: www.elsevier.com/locate/jpowsour

Rod-like hierarchical nano/micro $Li_{1.2}Ni_{0.2}Mn_{0.6}O_2$ as high performance cathode materials for lithium-ion batteries

Linjing Zhang [a], Borong Wu [a,b,*], Ning Li [a], Daobin Mu [a,b], Cunzhong Zhang [a,b], Feng Wu [a,b]

[a] School of Chemical Engineering and the Environment, Beijing Institute of Technology, Beijing Key Laboratory of Environmental Science and Engineering, Beijing 100081, China
[b] National Development Center of High Technology Green Materials, Beijing 100081, China

HIGHLIGHTS

- A rod-like hierarchical nano/micro $Li_{1.2}Ni_{0.2}Mn_{0.6}O_2$ is prepared by a hydrothermal method.
- A high discharge capacity of 266 mAh g^{-1} is retained by this material after 50 cycles at 0.1C-rate.
- It delivers a maximal capacity of 224 mAh g^{-1} and 214.3 mAh g^{-1} at 1C-rate and 2C-rate, respectively.
- Superior rate capability and cycleability are obtained attributed to the hierarchical nano/micro structures.

GRAPHICAL ABSTRACT

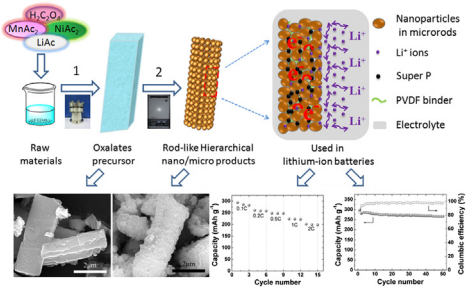

ARTICLE INFO

Article history:
Received 19 January 2013
Received in revised form
17 April 2013
Accepted 9 May 2013
Available online 17 May 2013

Keywords:
Hierarchical nano/micro
Hydrothermal
Rate capability
Cathode materials
Lithium-ion batteries

ABSTRACT

Rod-like hierarchical nano/micro structured lithium rich materials (RH-LNMO), $Li_{1.2}Ni_{0.2}Mn_{0.6}O_2$, have been synthesized using a facile hydrothermal method. The as-prepared samples are characterized by X-ray diffraction (XRD), filed emission scanning electron microscopy (FESEM) and transmission electron microscope (TEM). The rod-like hierarchical structures (1–3 μm in width and 3–10 μm in length) are assembled by nanoparticles with average sizes of 20–150 nm. Electrochemical data demonstrates that lithium cells using this lithium rich material as the cathode exhibit excellent performances. This material retains a high discharge capacity of 212.5 mAh g^{-1} (97% of the first discharge capacity) after 30 cycles at 1C-rate, and it yields an initial discharge capacity of 198 mAh g^{-1} at 2C-rate. The superior performance is attributed to the merits of the hierarchical nano/micro structures.

1. Introduction

Lithium-ion batteries (LIBs) as promising new energy sources play important roles in portable energy storage, hybrid electric vehicles (HEVs) and electric vehicles (EVs), because of their high energy density, high voltage and environmental benignity [1–4]. It is believed that the key to develop high performance rechargeable LIBs is the cathode material. However, low energy density of the conventional cathode materials, such as $LiCoO_2$, $LiFePO_4$ and $LiMO_2$ (M = Ni, Mn, Co), makes them less attractive for next-generation rechargeable LIBs [5–9]. As a result, developing high energy density cathode materials is still a great challenge.

Lithium rich layered oxides $xLi_2MnO_3 \cdot (1-x)LiNi_{1/2}Mn_{1/2}O_2$ have attracted significant attentions for use as promising cathode

* Corresponding author. School of Chemical Engineering and the Environment, Beijing Institute of Technology, Beijing Key Laboratory of Environmental Science and Engineering, Beijing 100081, China. Tel./fax: +86 10 6891 8828.
E-mail address: borongwu@gmail.com (B. Wu).

0378-7753/$ – see front matter © 2013 Elsevier B.V. All rights reserved.
http://dx.doi.org/10.1016/j.jpowsour.2013.05.019

materials owing to their much higher capacity (>250 mAh g^{-1}) with reduced cost [10–18]. Generally, these layered oxides are composed of two layered α-$NaFeO_2$-type structures [18,19]. There is Li_2MnO_3 domain within a predominant $LiNi_{1/2}Mn_{1/2}O_2$ layered phase that exists in these lithium rich materials. Taking advantages of each component, the most interesting feature of these lithium rich cathode materials is that they can be charged to a high potential (>4.5 V), where the conventional cathode materials are unstable, through the activation of Li_2MnO_3 component, thus yielding high capacities beyond 250 mAh g^{-1}. Although these layered oxides exhibit several merits, they suffer from intrinsic poor rate capability with modest cycle stability. The main reason is that lithium extraction is accompanied with the oxidation of O_{2p} band as a formula of Li_2O in the initial charge, followed by significant amounts of transition metal (TM) ions migration into the lithium sites. This irreversible migration will lead to a structural rearrangement at the surface of the lithium rich materials, thus hampering Li^+ mass transport [12,13,20].

Recently, various materials such as metallic compounds, polyaniline and single-walled carbon nanotubes, have been adopted to improve the electrochemical performance of lithium rich layered oxides [21–31]. But these methods cannot solve the inherent problems of these layered oxides as well. However, reducing the particle size to nanoscale levels has been considered to be an effective way to improve the rate capability of the layered oxides by shortening the lithium-ion diffusion pathways and increasing particles active surface areas [32–35]. For example, various nanowires and nanocrystalline lithium rich layered materials have been fabricated by many independent groups [36–39]. However, nanomaterials are usually thermodynamically unstable and tend to agglomerate, they are therefore difficult to realize uniform mixing with conductive additives. Hence, the high contact resistance of the electrode will induce capacity fading. The second disadvantage of nanomaterials is that high specific surface areas will promote side reactions between electrode and electrolyte, therefore leading to inferior cycling performance and poor safety. In order to find a solution for the poor capability of the lithium rich materials, one of the best strategies employed is to develop hierarchical nano/micro structures which are composed of nano-building blocks and micro-sized matrix. Lithium rich layered oxides of these structures are expected to reveal good performance because they can grasp both the advantages of nano and micro structures. While the former decreases the lithium diffusion lengths and is the key to favorable kinetics and high capacities, the latter promises low contact resistance, good structural stability and practical fabrication [40].

Herein, we propose a rational design of rod-like hierarchical nano/micro $Li_{1.2}Ni_{0.2}Mn_{0.6}O_2$ (RH-LNMO) cathode materials involving hydrothermal reaction followed by a calcination process. During the synthesis (as shown in Scheme 1), rod-like micro-sized matrixes are formed during the facile hydrothermal treatment, and the rod-like matrix is constructed of oxalates precursors. Sequentially, the oxalates precursors are decomposed accompanying with large amount of gas release during the calcination process, therefore, cubic or spherical shaped nanoparticles are formed and assembled in the rod-like matrix. At last, rod-like hierarchical nano/micro $Li_{1.2}Ni_{0.2}Mn_{0.6}O_2$ cathode materials are fabricated. This material combines the excellent rate capability conferred by the nanoparticles and good structural stability and cycling performance endowed by the main micro matrix.

2. Experimental

2.1. Synthesis of materials

The RH-LNMO materials were synthesized by a facile hydrothermal method combined with solid state calcination. All the raw materials were of analytical grade. The stoichiometric amounts of $Mn(CH_3COO)_2{\cdot}4H_2O$ and $Ni(CH_3COO)_2{\cdot}4H_2O$ were dissolved in distilled water. After stirring for a few minutes, $LiCH_3COO{\cdot}2H_2O$ and oxalic acid were added into the above solution separately and the solution turned to be slurry-like. The mixed slurry was continued stirring to be homogeneous and then transferred into a 100 mL Teflon-lined stainless steel autoclave. The autoclave was then sealed and maintained at a constant temperature of 180 °C for 2–12 h in an oven to obtain the precursor. Then the precursor was dried and subsequently preheated at 450 °C for 3–5 h, and thereafter calcined at 500 °C for 2–5 h, 750 °C for 2–5 h and 900 °C for 12–15 h in air.

2.2. Characterization

X-ray diffraction patterns of the hydrothermal precursors, as-prepared materials and electrochemical cycled electrodes were collected on a Rigaku Ultima IV-185 with Cu Kα radiation. The morphology was observed by field emission scanning electron microscopy (FESEM, FEI QUANTA 250). Transmission electron microscopy (TEM) and high-resolution transmission electron microscopy (HRTEM) were carried out on a JEOL 2011 instrument, equipped with energy X-ray (EDX) analysis. The chemical compositions of the as-synthesized materials were analyzed by inductively coupled plasma-atomic emission spectroscopy (ICP-AES, PROFILE SPEC). Thermal stability of the charged electrode was investigated by differential scanning calorimetry (DSC) on a NETZSCH DSC 404 F3 instrument when the electrode was charged to 4.6 V. In this experiment, the charged cell was opened in a glove box filled with argon and the cathode electrode was recovered from

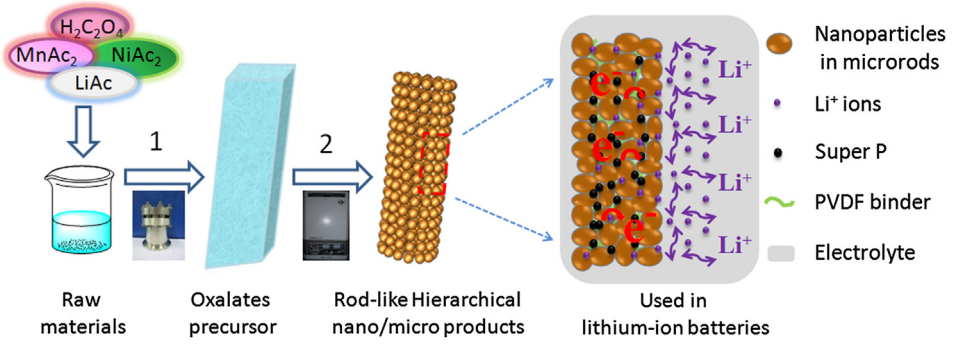

Scheme 1. Schematic illustration of the RH-LNMO materials preparation process and possible mechanisms for electrons and lithium-ions transport in lithium-ion batteries.

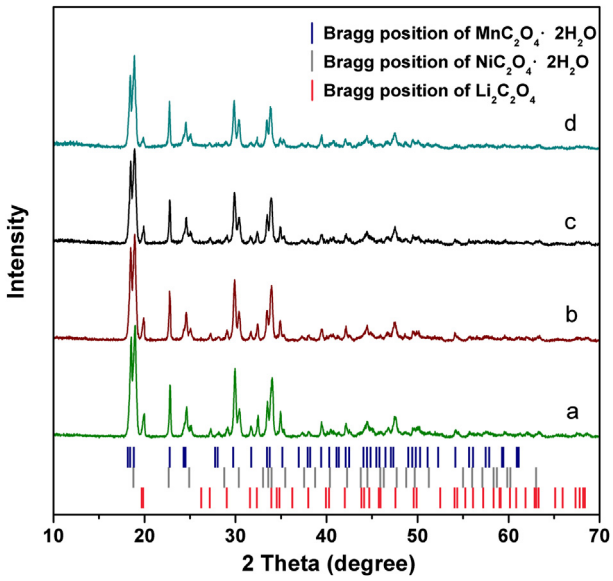

Fig. 1. XRD patterns of the precursors for different hydrothermal reaction time of the HR-LNMO materials: (a) 2 h; (b) 4 h; (c) 8 h; and (d) 12 h.

the cell. The DSC curve was carried out between 50 and 350 °C at a scan rate of 2 °C min^{-1}.

2.3. Electrochemical performance tests

Electrochemical performance of the RH-LNMO materials was performed using a coin-type cell (2025). The positive electrodes are consisted of lithium rich materials, Super P conductive carbon black and polyvinylidene difluoride (PVDF) in *N*-methyl-2-pyrrolidone (NMP) with a weight ratio of 80:10:10. The electrolyte was 1 M $LiPF_6$ dissolved in ethylene carbonate (EC)/dimethyl carbonate (DMC) mixture (1/1 *v*/*v*). The cells were assembled with lithium metals as the anodes in a glove box filled with argon. Galvanostatic charge and discharge tests were carried out on LAND (Wuhan, China) in the cut-off voltage between 4.8 and 2.0 V at 30 °C at various specific currents. Cyclic voltammograms (CVs; 2.0–5.0 V, 0.1 mV s^{-1}) measurements were performed on a CHI660D electrochemical workstation.

3. Results and discussion

3.1. Optimization of experimental conditions

The fabrication procedure of the hierarchical structured lithium rich materials is illustrated as shown in Scheme 1. In step 1, the raw materials are assembled into rod-like micro-sized matrix during the facile hydrothermal reaction, which is composed of oxalates precursors with dense surface. In step 2, the oxalates precursors are decomposed accompanied with gas release, generating lots of nanoparticles in the bulk matrix, and then the nanoparticles connect together via fusion of the edges of the particles.

The precursors of lithium rich cathode materials are prepared via a hydrothermal method under different reaction time for 2 h, 4 h, 8 h and 12 h. The crystal structure of the hydrothermal precursors is characterized by XRD patterns, which is shown in Fig. 1. All the peaks in the XRD patterns can be indexed to the characteristics based on $MnC_2O_4 \cdot 2H_2O$, $NiC_2O_4 \cdot 2H_2O$ and $Li_2C_2O_4$ phases. It is inferred that oxalates precursors are probably formed between acetates and oxalic acid during the hydrothermal process. The

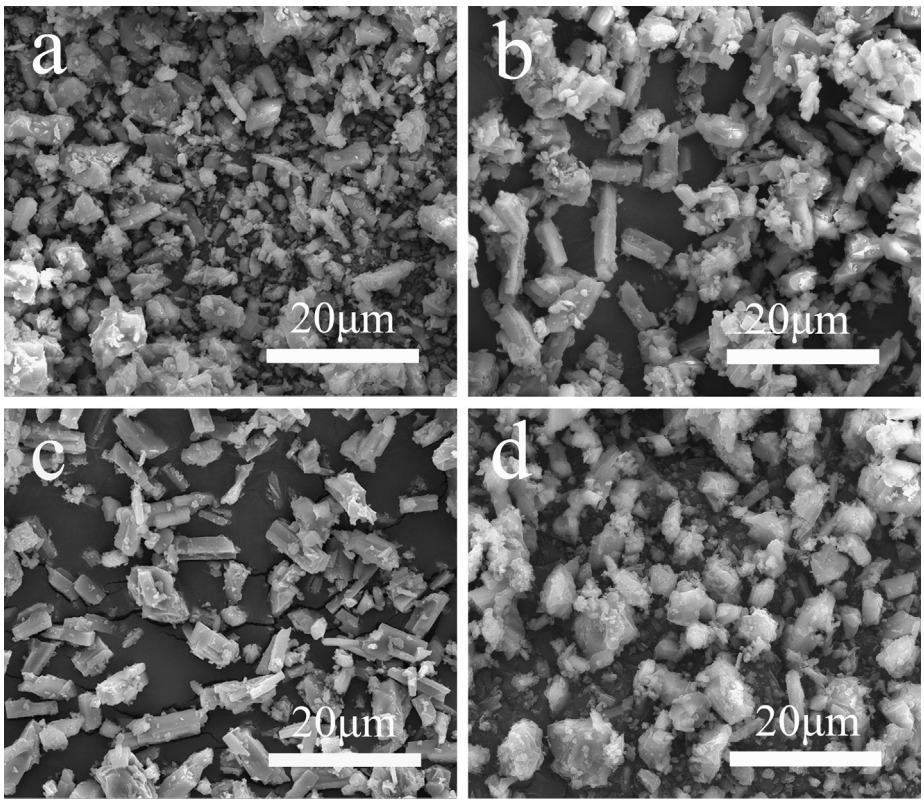

Fig. 2. Field emission scanning electron microscopy (FESEM) images of the oxalates precursors for different reaction time of the HR-LNMO materials: (a) 2 h; (b) 4 h; (c) 8 h; and (d) 12 h.

morphologies of the oxalates precursors are obtained by field emission scanning electron microscopy (FESEM). Obvious evolution stages can be observed when the reaction time increases from 2 to 12 h. In the initial stage, many colloids adhere together and form a certain amount of micro rods as shown in Fig. 2a and b. With the reaction time increasing to 8 h, it is clear that almost all the raw materials transform to micro-sized rods with various sizes ranging from 1 to 3 μm in width and 3 to 10 μm in length, as presented in Fig. 2c. Fig. 2d is FESEM image of the precursor reacted for 12 h, where one can see the micro rods aggregate together to form irregular blocks. Therefore, the sample reacted for 8 h is expected to yield desirable products with good structure and morphology.

Next, the precursors are calcined at high temperature, yielding lithium rich cathode materials. Table 1 provides the experimentally measured Li/Ni/Mn mole ratios determined by ICP-AES analysis for as-prepared products reacted for 2 h, 4 h, 8 h and 12 h. The data shows that little amount of lithium used is lost during high temperature sintering process. However, the experimentally measured Li/Ni/Mn mole ratios are approximately consistent with the ideal stoichiometry of $Li_{1.2}Ni_{0.2}Mn_{0.6}O_2$ due to the 5 wt.% excess lithium salt used in the initial synthesis. To investigate the structure characteristics of the products, XRD patterns are performed at a scan rate of $8^\circ\,min^{-1}$ as shown in Fig. 3. After calcination, most reflections of the XRD patterns can be indexed to the layered hexagonal α-$NaFeO_2$ structure (space group, $R\bar{3}m$), but the additional peaks observed around 36°, 44°, 58° and 64° (indicated by black asterisks) in the samples for 2 h, 4 h and 12 h have a strong similarity with the peaks of $LiMn_2O_4$ spinel ($Fd\bar{3}m$). However, the sample prepared for 8 h has a well-layered crystal structure, and the extended XRD patterns, morphology and electrochemical performance tests are carried out in the following work.

3.2. Extended structure and morphology analysis of RH-LNMO

To further investigate the fine structural characteristics of the as-prepared layered RH-LNMO powder for 8 h, the XRD patterns of the sample at a scan rate of $0.8^\circ\,min^{-1}$ are collected as shown in Fig. 4. It is clear that most of the reflections can be well indexed to a layered hexagonal α-$NaFeO_2$ structure (space group, $R\bar{3}m$). The other weak peaks between 20 and 23° indicated by the black rectangle are the characteristics of the Li_2MnO_3 component with relatively low symmetry (Monoclinic, $C2/m$), originating from superlattice ordering of the Li and Mn in the transition metal layer. No impurities are detected in the whole patterns, implying the high purity of the layered oxides. Moreover, the well splitting of both the (006)/(012) and the (018)/(110) peaks indicates the well-defined layered structure of the RH-LNMO material. The intensity ratio of the $I_{(003)}/I_{(104)}$ peaks in the XRD patterns is usually regarded as the degree of the cation mixing in the Li-layers of the layered materials. The $I_{(003)}/I_{(104)}$ value of the RH-LNMO material is 1.22, suggesting the good layered structure and negligible

Table 1
The experimentally measured Li/Ni/Mn mole ratio for as-prepared products reacted for 2 h, 4 h, 8 h and 12 h. The oxygen content has been normalized to a stoichiometry of 2.

Sample	Measured stoichiometry (Ref. O = 2)			
	Li	Ni	Mn	O
Ideal value	1.200	0.200	0.600	2
2 h	1.212	0.201	0.596	2
4 h	1.207	0.198	0.601	2
8 h	1.214	0.198	0.599	2
12 h	1.211	0.202	0.595	2

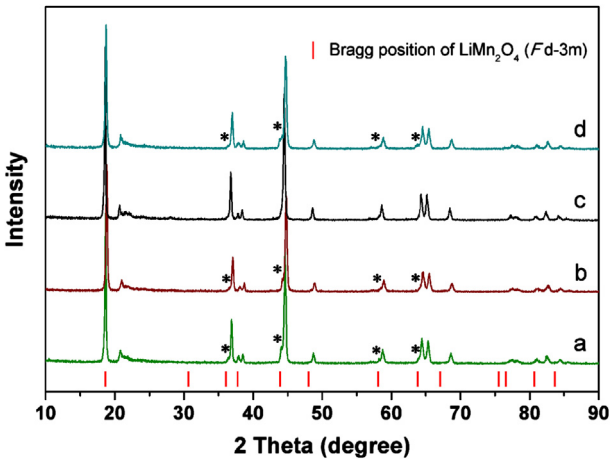

Fig. 3. XRD patterns of the as-prepared RH-LNMO materials for different reaction time: (a) 2 h; (b) 4 h; (c) 8 h; and (d) 12 h. The scan rate is $8^\circ\,min^{-1}$.

disordered arrangement of Li and Ni ions in the synthesized RH-LNMO material.

Fig. 5 shows the field emission scanning electron microscopy (FESEM) images of the precursor and the as-prepared RH-LNMO powder material under different magnifications. Fig. 5a provides the clear evidence of micron rod-like structures of oxalates precursors with dense surface. After calcination, the dense micro rod-like particle develops hierarchical nano/micro structure, and no obvious changes are observed in particle sizes as shown in the FESEM image in Fig. 5b. Fig. 5c shows the magnified rod-like hierarchical nano/micro structures of the as-prepared products, which are assembled by lots of cubic or spherical-like nanoparticles with a size ranging from 20 to 150 nm. Therefore, these small nanoparticles favor facile lithium-ion diffusions through shortened distance, which are expected to enhance the rate performance of the material. Furthermore, there seems to have tiny voids between nanoparticles due to gas release during decomposition of oxalates, which may accelerate the electrolyte penetration. Also, the hierarchical nano/micro rods enable to reduce side reactions between electrode and electrolyte due to the relatively low surface areas as the nanoparticles are not completely isolated, which have the potential to improve the cycling performance of the material.

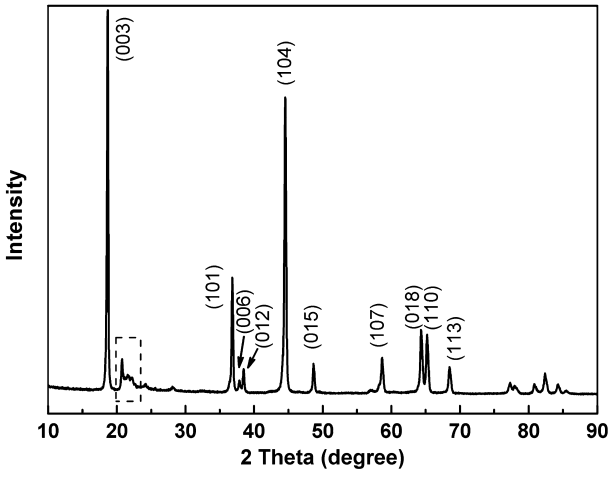

Fig. 4. XRD patterns of the as-prepared layered RH-LNMO materials. The scan rate is $0.8^\circ\,min^{-1}$.

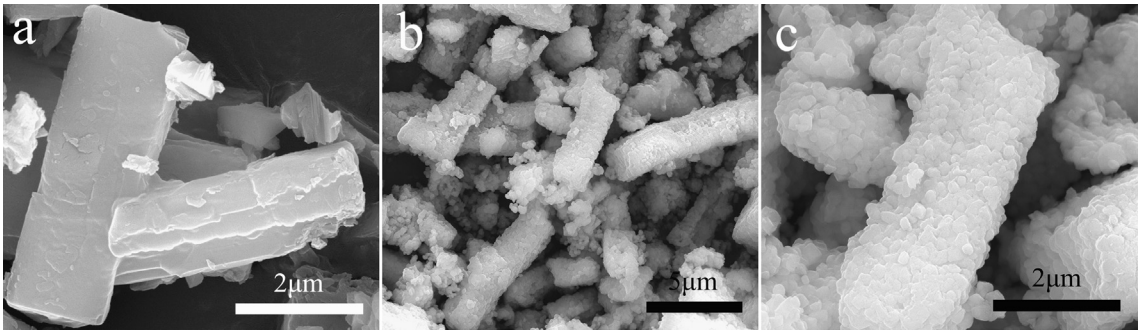

Fig. 5. Field emission scanning electron microscopy (FESEM) images of (a) oxalates precursor; and (b–c) as-prepared RH-LNMO material under different magnifications.

The as-prepared RH-LNMO layered cathode materials are further investigated by transmission electron microscopy (TEM) and high-resolution transmission electron microscopy (HRTEM) as shown in Fig. 6. From the typical TEM image in Fig. 6a, we can see the RH-LNMO materials yield obvious rod-like morphology, which is consistent with the FESEM results in Fig. 5b. Magnified TEM image of the RH-LNMO is shown in Fig. 6b, which confirms that the rod-like hierarchical nano/micro structures are composed of plenty of conjunctive nanoparticles. Fig. 6c exhibits the HRTEM image of an individual nanoparticle from the selected area in Fig. 6b. Apparent lattice fringes can be observed and the width of 0.47 nm between lattice fringes is consistent with the interspacing of (003) planes in lithium rich layered materials, which agrees well with the XRD analysis results. Energy-dispersive X-ray analysis (EDX) confirms the presence of both Mn and Ni elements in RH-LNMO materials as shown in Fig. 6d.

3.3. Cycling performance and structural stability

The electrochemical performances of lithium cells with RH-LNMO cathode materials are investigated using coin-type half cells. Fig. 7a illustrates the charge and discharge profiles of the RH-LNMO electrodes cycled between 4.8 and 2.0 V at a specific current of 25 mA g^{-1} (0.1C-rate). The RH-LNMO material delivers initial

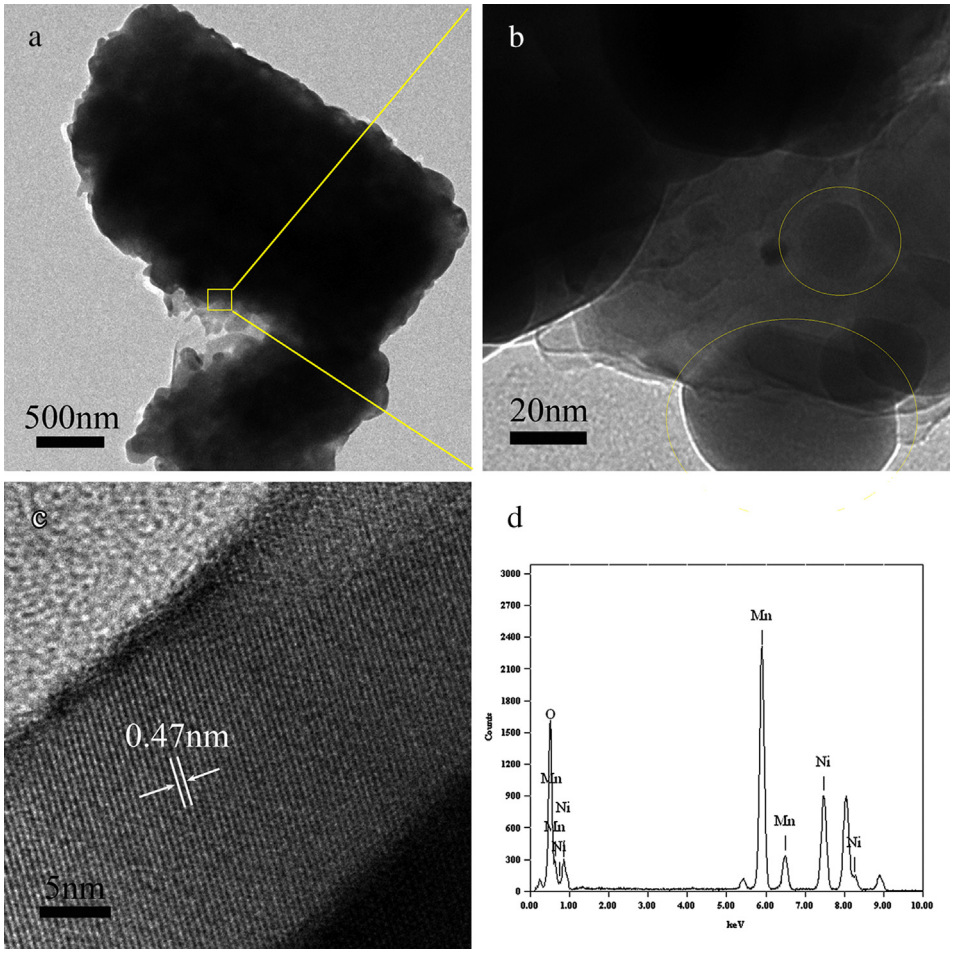

Fig. 6. (a) TEM image of RH-LNMO; (b) TEM image of the nanoparticles from (a); (c) high-resolution TEM image; and (d) EDX pattern.

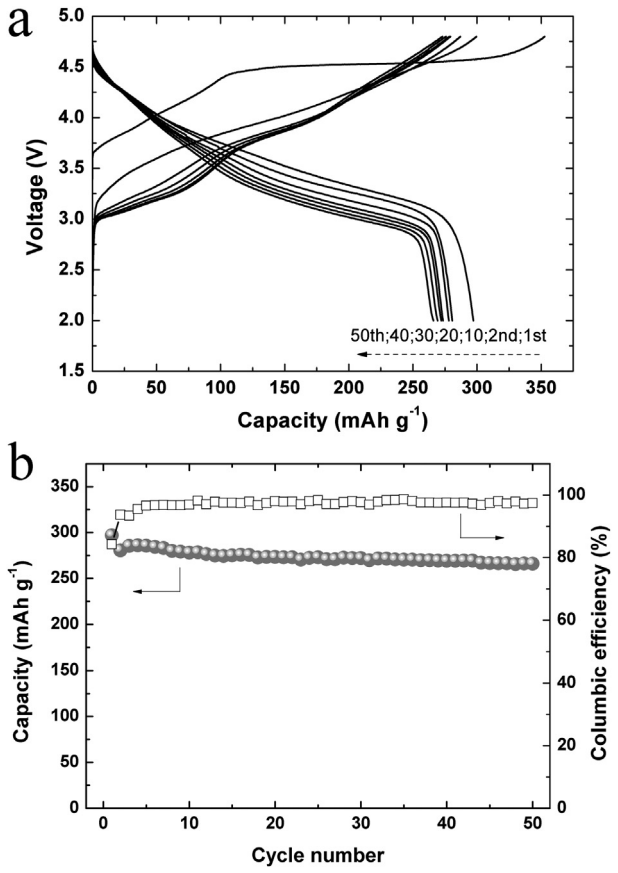

Fig. 7. (a) Voltage profiles; and (b) capacity retention *vs.* cycle number of the RH-LNMO electrodes, cycled between 4.8 and 2.0 V at a specific current of 25 mA g^{-1}.

charge/discharge capacities of 352.8 mAh g^{-1} and 297.1 mAh g^{-1}, respectively, which are among the best in previous reports [11,16,27,32,41]. The capacity retention *vs.* cycle number of the RH-LNMO electrode is shown in Fig. 7b. As one can see that at the completion of 50th cycles, a high discharge capacity of 266 mAh g^{-1} is maintained, indicating the good cycling performance of the RH-LNMO material. Furthermore, the columbic efficiency is about 98% after initial several cycles shown in Fig. 7b. It is inferred that this improved electrochemical performance in terms of charge/discharge capacity and cycling for the RH-LNMO material is linked to the structural stability of the rod-like hierarchical nano/micro structures, which will be illustrated later.

Cycle voltammograms (CVs) of the RH-LNMO materials are recorded at a sweep rate of 0.1 mV s^{-1} between 5.0 and 2.0 V (Fig. 8) to gather information about the individual redox process that occurs during charge and discharge. In the CVs, the first anodic peak around 4.0 V on the initial cycle is predominantly associated with Ni oxidation from Ni^{2+} to Ni^{4+}, and the second anodic peak at higher potential (~4.5–4.7 V) is predominantly attributed to the irreversible electrochemical activation reaction that extracts Li_2O from Li_2MnO_3 component to form MnO_2 [33,42]. Two cathodic peaks at ~4.5–3.25 V are observed on discharge, which are associated with reduction of Ni and Mn. It is evident that both reaction processes are reversible in the 2nd and the 3rd cycles, and almost overlap between the two cycle profiles indicates the good reversibility of the RH-LNMO materials.

To further demonstrate the origins for the good cycling performance of the RH-LNMO materials, *ex situ* XRD patterns of the charged/discharged electrodes are characterized shown in Fig. 9a. No obvious phase transformation is observed on charging to 4.8 V,

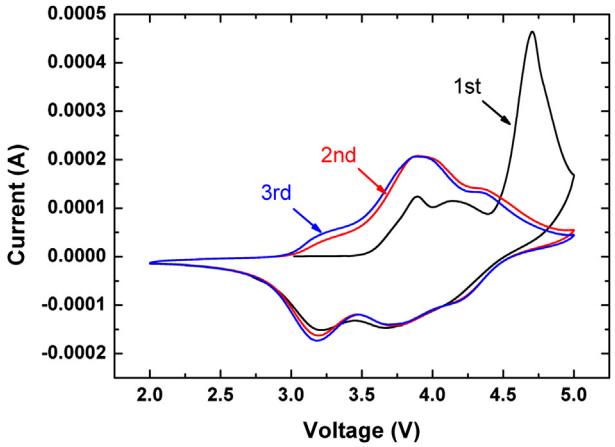

Fig. 8. Cycle voltammograms of the RH-LNMO materials, cycled between 5.0 and 2.0 V at a sweep rate of 0.1 mV s^{-1}.

and all the diffraction patterns of the RH-LNMO can still be indexed with a layered structure, in spite of the most lithium removal from the materials. However, the superlattice peaks between 20 and 23° show a remarkable decrease compared with the pristine RH-LNMO, which is associated with loss of the $LiMn_6$ ordering in the transition metal layers. The XRD patterns of the initially discharged electrode can also be indexed with a layered structure, indicating the structural stability of the RH-LNMO material. Note that the structural integrity is preserved and no obvious phase transformation is observed in the patterns of 50th cycled electrode. Therefore, we can safely conclude that what contributes to the excellent cycling performance is the good structural stability of the main micro structure of the RH-LNMO materials.

Fig. 9b shows the differential capacity *vs.* voltage profiles for the RH-LNMO electrodes, which are cycled between 4.8 and 2.0 V at 0.1C-rate. The sharp peak around 4.5 V is associated with the irreversible Li_2O removal from the Li_2MnO_3 component which is consistent with Fig. 7a. Note that there is a reduction peak around 3.25 V in the initial discharge curve, which is corresponding to the Mn^{3+}/Mn^{4+} redox couple. In the following cycles, the redox couple peaks around 3.25 V become close to 3.0 V. The limited voltage shift in reduction peaks is likely due to the increase of inner resistance [11,12]. The inset of the Fig. 9b shows the d*Q*/d*V* profiles for the RH-LNMO electrodes cycled at 1C-rate. The reduction peaks corresponding to the Mn^{3+}/Mn^{4+} redox couple also retain around 3.0 V from 10th to 30th cycles, and the voltage variation tendency is similar to that at 0.1C-rate. Fig. 9c and d provides the field emission scanning electron microscopy (FESEM) images of the 50th cycled electrode. As one can see that the rod-like structures are still preserved after the electrode experiences 50 cycles. Consequently, we can further conclude that the excellent cycling performance is obtained due to the intrinsic good structural stability of the hierarchical nano/micro structure materials.

3.4. Rate capability

The rate performance of the RH-LNMO materials is shown in Fig. 10a. All the cells are charged at 0.1C-rate to reduce polarization and discharged at 0.2, 0.5, 1 and 2C-rates, respectively. The initial discharge capacities of RH-LNMO electrodes are 260.8, 247.8, 219.6 and 198 mAh g^{-1} at 0.2, 0.5, 1 and 2C discharge rates. The IR drop associated with increased inner resistance of the cells is obviously seen from the 0.2, 0.5, 1 and 2C discharge curves. However, the high rate discharge capacities indicate the excellent rate performance for this RH-LNMO cathode material. Fig. 10b shows the capacity

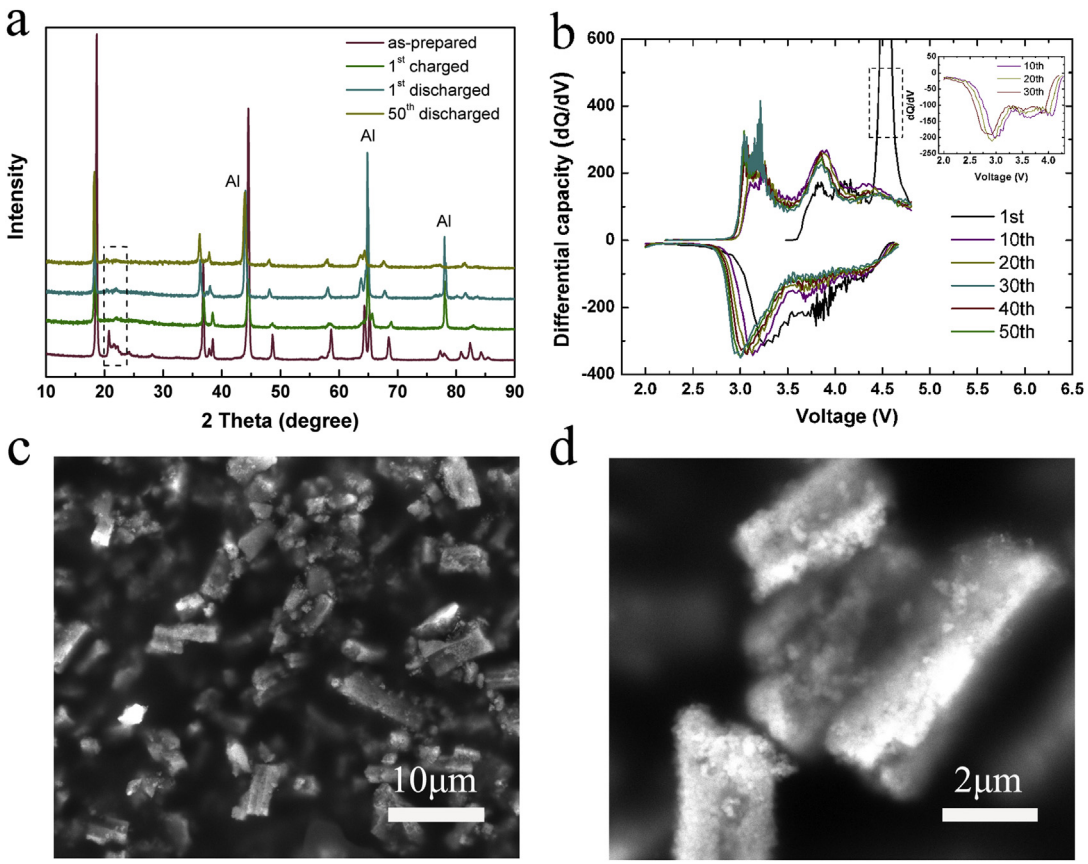

Fig. 9. (a) XRD patterns of the as-prepared RH-LNMO powder, fully charged, fully discharged and multiple cycled electrodes. All the electrodes are cycled at 25 mA g^{-1}; (b) differential capacity *vs.* voltage profiles of the RH-LNMO materials, cycled between 4.8 and 2.0 V at 25 mA g^{-1}. The inset of Fig. 9b is the d*Q*/d*V* profiles of the RH-LNMO electrodes cycled at 250 mA g^{-1}; (c–d) FESEM images of the electrode after 50 cycles under different magnifications.

retention *vs.* cycle number profiles for RH-LNMO electrodes cycled under the same conditions with that in Fig. 10a. Surprisingly, it yields a maximal discharge capacity of 224 and 214.3 mAh g^{-1} at 1C- and 2C-rates, due to further activation of the Li_2MnO_3 component at high rates. Furthermore, high discharge capacities of 244.2, 225.5, 212.5 and 186.2 mAh g^{-1} can be maintained at the completion of 30 cycles at 0.2, 0.5, 1 and 2C-rates, and the capacity retentions are 94%, 91%, 97% and 94% of the initial discharge capacities, respectively, indicating the outstanding rate cycling performance of the RH-LNMO material.

To further evaluate the performance of the RH-LNMO electrodes at high rates, the discharge capacities as a function of specific currents are presented in Fig. 11. The cells are charged at a constant rate of 0.1C, and then discharged at 0.1, 0.2, 0.5, 1 and 2C-rates between 4.8 and 2.0 V with 3 cycles per step. The initial discharge capacities at low rates are above 250 mAh g^{-1}, decreasing gradually

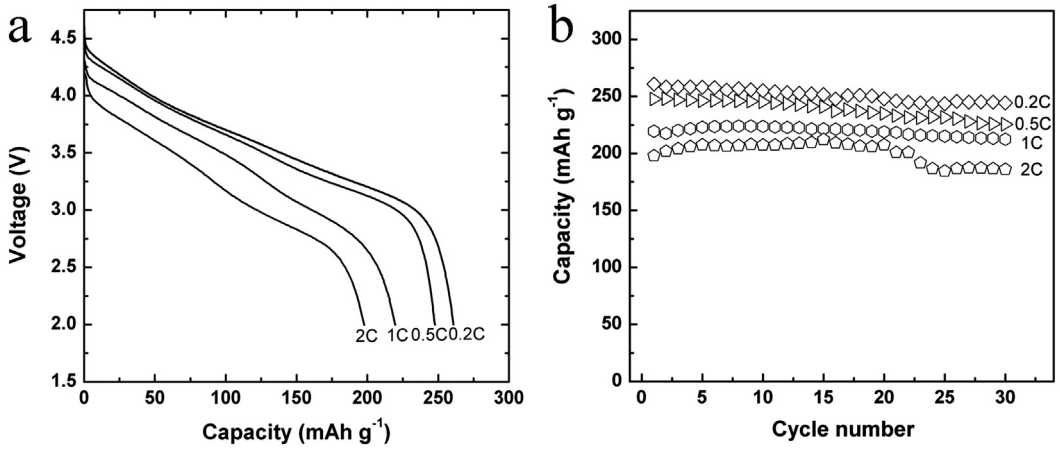

Fig. 10. (a) Initial discharge voltage profiles; and (b) capacity retention *vs.* cycle number of the RH-LNMO electrodes, cycled between 4.8 and 2.0 V at various specific currents ranging from 25 to 500 mA g^{-1}.

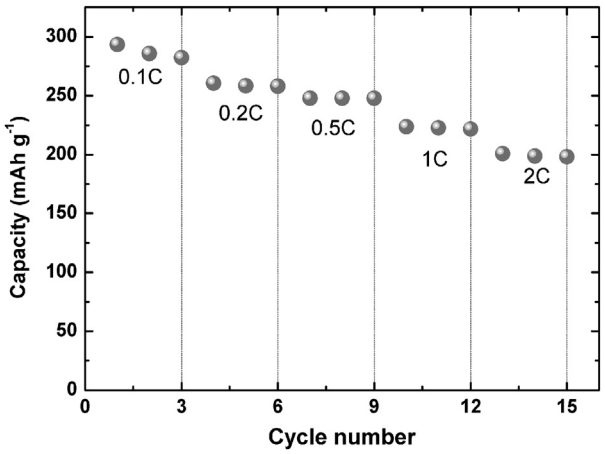

Fig. 11. Rate capability of the RH-LNMO electrodes, cycled between 4.8 and 2.0 V at specific currents from 25 to 500 mA g^{-1} for 3 cycles per step. All the cells are charged at 25 mA g^{-1}.

due to the increasing current densities. However, high specific capacities are achieved at 1C- and 2C-rates, and reversible capacities can be preserved after 3 cycles, indicating the excellent rate performance of the RH-LNMO material. The excellent rate capability is mainly attributed to the rod-like hierarchical nano/micro structures, which facilitate electrons transfer and lithium-ions diffusion in the bulk materials. The nanoparticles in the hierarchical nano/micro structures enable to shorten diffusion length, implying far higher lithium-ion intercalation/deintercalation rates and faster electron transport. The hierarchical nano/micro structures can also accelerate electrolyte penetration into each nanoparticle through tiny voids derived from decomposition of oxalates precursors, thus ensuring good contact between electrolyte and cathode materials. Moreover, the good structural stability endowed by the main micro rod-like structure may also contribute to the excellent rate capability of the RH-LNMO materials.

3.5. Thermal stability

When cathode materials are being considered for applications in commercial energy storage systems, HEVs and EVs, the thermal stability of these materials is of significant importance. Fig. 12 shows the differential scanning calorimetry (DSC) curve of the RH-LNMO electrode charged to 4.6 V. The RH-LNMO cathode material exhibits the major exothermal peak at 259.8 °C with the overall heat generation of 995.5 J g^{-1}. The high exothermal temperature indicates the good structural stability and safety characteristics of the RH-LNMO samples compared with the materials in previous report [10]. The good thermal stability is attributed to the hierarchical nano/micro structures composed of incompletely isolated nanoparticles with relatively high thermodynamic stability. This novel structure reduces the side reactions between cathode materials and electrolyte, thus improving their safety performance compared with that of individual nanoparticles.

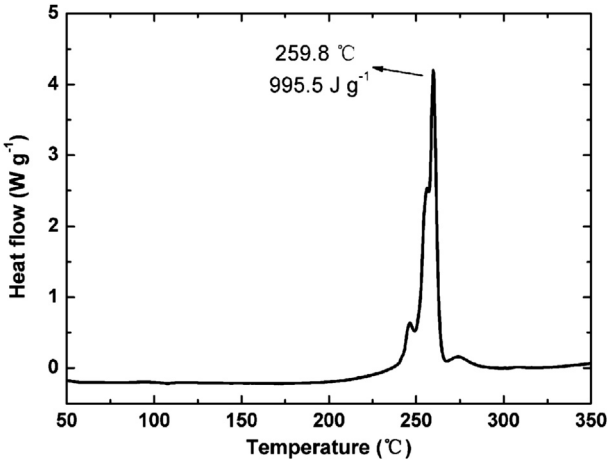

Fig. 12. DSC profiles of the RH-LNMO electrodes which are charged to 4.6 V. The scan rate is 2 °C min^{-1}.

4. Conclusion

In conclusion, the rod-like hierarchical nano/micro $Li_{1.2}Ni_{0.2}Mn_{0.6}O_2$ materials have been successfully synthesized via a facile hydrothermal method combined with calcination process. It manifests excellent performance in terms of discharge capacities, rate and cycling. The excellent performance of the RH-LNMO materials is mainly ascribed to the hierarchical nano/micro structures, as well as good structural stability. In this structure, nanoparticles provide short diffusion lengths which favor rapid lithium-ions insercalation/deinsercalation rates and fast electrons transfer, and the micro matrix supports a main structure with good thermodynamic stability. Thus, the hierarchical nano/micro $Li_{1.2}Ni_{0.2}Mn_{0.6}O_2$ materials may be promising candidates for cathode materials of high performance lithium-ion batteries. The methodology of preparing RH-LNMO materials can also be employed to synthesize other derivative layered oxides or lithium manganese nickel oxides with spinel structures, even those materials used in other fields such as super capacitors and catalysts. In addition, kinds of derivative structures combined nanoparticles with micro particles can be developed according to varied requirements based on this hierarchical nano/micro technology.

Acknowledgments

This work was supported by Ministry of Science and Technology (MOST) of China (2010DFA72760), US–China Collaboration on cutting-edge technology development of electric vehicle and the National Science Foundation of China (11076003).

References

[1] J.-M. Tarascon, M. Armand, Nature 414 (2001) 359.
[2] M. Armand, J.-M. Tarascon, Nature 451 (2008) 652.
[3] K. Kang, Y.S. Meng, J. Bréger, C.P. Gray, G. Ceder, Science 311 (2006) 977.
[4] Y.-K. Sun, S.-T. Myung, B.-C. Park, J. Prakash, I. Belharouak, K. Amine, Nat. Mater. 8 (2009) 320.
[5] B. Scrosati, J. Garche, J. Power Sourc. 195 (2010) 2419.
[6] A.K. Padhi, K.S. Nanjundaswamy, J.B. Goodenough, J. Electrochem. Soc. 144 (1997) 1188.
[7] K. Dokko, S. Koizumi, H. Nakanob, K. Kanamura, J. Mater. Chem. 17 (2007) 4803.
[8] K. Saravanan, M.V. Reddy, P. Balaya, H. Gong, B.V.R. Chowdari, J.J. Vittal, J. Mater. Chem. 19 (2009) 605.
[9] V. Etacheri, R. Marom, R. Elazari, G. Salitra, D. Aurbach, Energy Environ. Sci. 4 (2011) 3243.
[10] Z. Lu, D.D. MacNeil, J.R. Dahn, Electrochem. Solid State Lett. 4 (2001) A191.
[11] Z. Lu, L.Y. Beaulieu, R.A. Donaberger, C.L. Thomas, J.R. Dahn, J. Electrochem. Soc. 149 (2002) A778.
[12] Z. Lu, J.R. Dahn, J. Electrochem. Soc. 149 (2002) A815.
[13] A.R. Armstrong, M. Holzapfel, P. Novák, C.S. Johnson, S.-H. Kang, M.M. Thackeray, P.G. Bruce, J. Am. Chem. Soc. 128 (2006) 8694.
[14] B. Ammundsen, J. Paulsen, Adv. Mater. 13 (2001) 943.
[15] C.S. Johnson, N. Li, C. Lefief, M.M. Thackeray, Electrochem. Commun. 9 (2007) 787.
[16] Y.-S. Hong, Y.J. Park, K.S. Ryu, S.H. Changa, M.G. Kim, J. Mater. Chem. 14 (2004) 1424.
[17] M.M. Thackeray, C.S. Johnson, J.T. Vaughey, N. Li, S.A. Hackney, J. Mater. Chem. 15 (2005) 2257.

[18] C.H. Lei, J. Bareño, J.G. Wen, I. Petrov, S.-H. Kang, D.P. Abraham, J. Power Sourc. 178 (2008) 422.
[19] J.-S. Kim, C.S. Johnson, J.T. Vaughey, M.M. Thackeray, Chem. Mater. 16 (2004) 1996.
[20] B. Xu, C.R. Fell, M. Chi, Y.S. Meng, Energy Environ. Sci. 4 (2011) 2223.
[21] W.C. West, J. Soler, M.C. Smart, B.V. Ratnakumar, S. Firdosy, V. Ravi, M.S. Anderson, J. Hrbacek, E.S. Lee, A. Manthiram, J. Electrochem. Soc. 158 (2011) A883.
[22] J. Liu, B. Reeja-Jayan, A. Manthiram, J. Phys. Chem. C 114 (2010) 9528.
[23] Q.Y. Wang, J. Liu, A.V. Murugan, A. Manthiram, J. Mater. Chem. 19 (2009) 4965.
[24] J. Gao, J. Kim, A. Manthiram, Electrochem. Commun. 11 (2009) 84.
[25] Y. Wu, A. Manthiram, Solid State Ionics 180 (2009) 50.
[26] J. Liu, A. Manthiram, J. Mater. Chem. 20 (2010) 3961.
[27] Y.-J. Kang, J.-H. Kim, S.-W. Lee, Y.-K. Sun, Electrochim. Acta 50 (2005) 4784.
[28] D. Ahn, Y.-M. Koo, M.G. Kim, N. Shin, J. Park, J. Eom, J. Cho, T.J. Shin, J. Phys. Chem. C 114 (2010) 3675.
[29] C. Ban, Z. Li, Z. Wu, M.J. Kirkham, L. Chen, Y.S. Jung, E.A. Payzant, Y. Yan, M.S. Whittingham, A.C. Dillon, Adv. Energy Mater. 1 (2011) 58.
[30] F. Wu, N. Li, Y. Su, H. Lu, L. Zhang, R. An, Z.W.L.Y. Bao, S. Chen, J. Mater. Chem. 22 (2012) 1489.
[31] Y.-K. Sun, M.-J. Lee, C.S. Yoon, J. Hassoun, K. Amine, B. Scrosati, Adv. Mater. 24 (2012) 1192.
[32] D. Wang, I. Belharouak, G. Zhou, K. Amine, Adv. Funct. Mater. 23 (2013) 1070.
[33] P.-C. Chen, M.-C. Tsai, H.-C. Chen, I.-N. Lin, H.-S. Sheu, Y.-S. Lin, J.-G. Duh, H.-T. Chiu, C.-Y. Lee, J. Mater. Chem. 22 (2012) 5349.
[34] S. Ding, X.W. (David) Lou, Nanoscale 3 (2011) 3586.
[35] P. Si, S. Ding, J. Yuan, X.W. (David) Lou, D.-H. Kim, ACS Nano 5 (2011) 7617.
[36] L. Yu, H. Yang, X. Ai, Y. Cao, J. Phys. Chem. B 109 (2005) 1148.
[37] M.G. Kim, M. Jo, Y.-S. Hong, J. Cho, Chem. Commun. 2 (2009) 218.
[38] W. He, J. Qian, Y. Cao, X. Ai, H. Yang, RSC Adv. 2 (2012) 3423.
[39] J. Liu, L. Chen, M. Hou, F. Wang, R. Che, Y. Xia, J. Mater. Chem. 22 (2012) 25380.
[40] Y.-G. Guo, J.-S. Hu, L.-J. Wan, Adv. Mater. 20 (2008) 2878.
[41] D.-K. Lee, S.-H. Park, K. Amine, H.J. Bang, J. Parakash, Y.-K. Sun, J. Power Sourc. 162 (2006) 1346.
[42] C.S. Johnson, N. Li, C. Lefief, J.T. Vaughey, M.M. Thackeray, Chem. Mater. 20 (2008) 6095.